Interannual Variability of Monsoon Precipitation and Local Subcloud Equivalent Potential Temperature

JOHN V. HURLEY AND WILLIAM R. BOOS

Department of Geology and Geophysics, Yale University, New Haven, Connecticut

ABSTRACT

The interannual variability of monsoon precipitation is described in the context of a convective quasi-equilibrium framework. Using two reanalysis products and two global precipitation datasets, the authors examine linear relationships between seasonal anomalies of precipitation and subcloud equivalent potential temperature (θ_{eb}) local to six monsoon regions. This approach provides a single near-surface thermodynamically relevant variable over both land and ocean, extending previous studies of interannual monsoon variability that emphasized ocean surface temperatures. After removing the variability linearly associated with an index of the El Niño–Southern Oscillation, positive monsoon precipitation anomalies are shown to be associated with enhanced θ_{eb} local to and slightly poleward of the climatological θ_{eb} maximum. The variations in continental θ_{eb} local to the monsoon precipitation maxima are mainly due to variations in subcloud specific humidity, with changes in subcloud temperature having the opposite sign. Motivated by the fact that some of these subcloud humidity anomalies occur over deserts poleward of monsoon regions, the relationship of 700-hPa flow with precipitation is examined, and enhanced precipitation in several regions is found to covary with the properties of shallow meridional circulations. The implications of these results for the understanding of monsoon interannual variability are discussed.

1. Introduction

Earth's seasonal cycle of insolation drives monsoon circulations only indirectly, with ocean and land surfaces absorbing most shortwave radiation before transferring the energy of that radiation to the overlying atmosphere via turbulent heat fluxes. It is thus no surprise that variations in the strength of monsoons have, for over a century, been associated with changes in the properties of land and ocean surfaces. For example, Blanford (1884) suggested that unusually heavy Himalayan snowfall led to drought over northwestern India, and Charney (1975) argued, in the context of the Sahel, that reductions in vegetation could increase land surface albedo and enhance atmospheric subsidence in a positive feedback. Both of these ideas relate monsoon precipitation to land–atmosphere interaction near the poleward edge of the monsoon domain.

Attention in recent years has shifted from the influence of land surface properties to the covariation of sea surface temperature (SST) with monsoon precipitation, so that SST changes are often considered to be the leading cause of monsoon interannual variability (Rasmusson and Carpenter 1983; Yang and Lau 2004). A decades-long drought in the Sahel has been linked not to Africa's surface albedo but to changes in tropical SST (Biasutti et al. 2008; Giannini et al. 2003; Hoerling et al. 2006; Lu 2009). Australian monsoon activity is strongly correlated with Pacific SST (Taschetto et al. 2009, 2010), and interannual variations in South Asian precipitation are associated with SST changes in both the El Niño–Southern Oscillation (ENSO; Li et al. 2007; Shukla and Paolino 1983) and an east–west Indian Ocean dipole (IOD; Saji et al. 1999; Webster et al. 1999).

But even SST variations associated with ENSO, which have an especially strong relationship with rainfall in the South Asian and Australian monsoons, are linearly related to less than half of the interannual variance of precipitation in those regions (Webster et al. 1998). This is perhaps expected since monsoons are thought to be caused by a contrast in the thermal forcing between land and ocean, and land surface thermal forcing is likely at least somewhat independent of SST. When attempting to assess the state of a monsoon's forcing, one is thus in

Corresponding author address: John V. Hurley, Department of Geology and Geophysics, Yale University, 210 Whitney Ave., New Haven, CT 06511.
E-mail: jvhurley12@gmail.com

the position of trying to combine the SST field with some physically relevant measure of land surface properties. Land surface temperature, although well observed, is largely unrelated to the strength of monsoon circulations, in which the phase changes of atmospheric water play a first-order thermodynamic role (Fasullo and Webster 2003). Blanford's hypothesized relation between Himalayan snow cover and Indian precipitation has not been verified in observations (Robock et al. 2003), and the influence of soil moisture on monsoon precipitation exhibits substantial regional variation and is difficult, at best, to assess observationally (Douville et al. 2001; Godfred-Spenning and Reason 2002). While previous studies have used numerical models to examine the sensitivity of monsoon precipitation to snow cover, soil moisture, surface albedo, and other parameters (Douville et al. 2001; Vernekar et al. 1995), we know of no variable representing the state of a land surface that has been shown to be strongly correlated with observed interannual variations of precipitation in multiple monsoon regions.

The goal of this paper is to examine the covariation of monsoon precipitation with a near-surface thermodynamic variable that is relevant over both land and ocean. We employ the framework of convective quasi equilibrium (QE), in which precipitating convection is hypothesized to consume convective available potential energy (CAPE) fast enough for any changes in CAPE to be small compared to the rate of generation of CAPE by radiative cooling and surface heat fluxes (Arakawa and Schubert 1974; Emanuel et al. 1994; Neelin et al. 2008). In a strict form of QE, any changes in CAPE are assumed to be dynamically negligible, so that temperatures within the convecting layer follow a moist adiabat tied to the equivalent potential temperature of air below the base of cumulus clouds (θ_{eb}). This strict form of QE is theoretically attractive because it dramatically simplifies the vertical structure of the troposphere and ties it to a single near-surface variable, but it is clear that this is an oversimplification for many tropical atmospheric phenomena (Arakawa 2004; Brown and Bretherton 1997). Nevertheless, strict forms of QE have been used in numerous theoretical studies of monsoon dynamics (Boos and Emanuel 2008b; Chou et al. 2001; Neelin 2007; Prive and Plumb 2007a,b) and have been shown to provide a decent description of the seasonal-mean state of some observed monsoons (Nie et al. 2010). In particular, Nie et al. (2010) showed that maxima of θ_{eb} in many of Earth's regional monsoons are located in the same positions as maxima of upper-tropospheric temperature (T_u). This coincidence of maxima of θ_{eb} and T_u is expected if moist convection couples those two variables only in a narrow monsoonal convergence zone located near the thermal maximum; moist convection and thus

the coupling between θ_{eb} and T_u are suppressed in the broad subsiding branch of the overturning circulation that occupies the rest of the domain.

Since θ_{eb} and T_u appear to be related in this relatively simple way in seasonal climatologies of observed monsoons, it seems reasonable to ask if something can be learned by examining the interannual variations of these variables. More precisely, are interannual variations in θ_{eb} linearly related to interannual variations in monsoon precipitation? And does T_u covary in a similar fashion? Values of θ_{eb} will be closely tied to local SST over the ocean, although they can vary independently of SST if subcloud relative humidity and air–sea temperature difference are not constant. Over land, θ_{eb} is less constrained and likely has less persistence than SST. One thus cannot regard θ_{eb} as a lower boundary condition for monsoon flow, but examination of its interannual variations may nevertheless help in understanding the processes governing monsoon variability. In particular, since θ_{eb} is defined over both land and ocean, it allows monsoon variability to be assessed in a simple theoretical framework in which the thermodynamic state of near-surface air is represented by a single variable throughout the entire domain.

This is the first study, as far as we know, that examines covariations between precipitation in multiple monsoon regions and equivalent potential temperature on a terrain-following surface in the subcloud layer. While detailed exploration of the mechanisms responsible for these covariations is left for future work, we do have a general hypothesis that a monsoon circulation and its associated precipitation will be stronger when the meridional gradient of θ_{eb} is stronger (Emanuel 1995). Strengthening of the meridional gradient may occur through increased θ_{eb} at the location of the θ_{eb} maximum in the summer hemisphere or by reduced θ_{eb} near the equator or in the winter hemisphere. This positive relationship between monsoon precipitation and the meridional gradient of θ_{eb} was illustrated clearly by Eltahir and Gong (1996), using observations of boundary layer moist entropy for one wet and one dry year (1958 and 1960, respectively) of the West African monsoon. The present work can thus be regarded as an extension of Eltahir and Gong (1996) to six monsoon regions using a much longer observational record.

Like Eltahir and Gong (1996), we find that monsoon precipitation does covary interannually with θ_{eb}. But unlike their work, which focused on the meridional gradient of θ_{eb} between the precipitation maximum and the equatorial ocean, we show that a robust feature across all six monsoon regions is the covariation of monsoon precipitation with continental θ_{eb} near and somewhat poleward of the climatological maxima of precipitation

and θ_{eb}. For this reason, the scope of this manuscript is limited to the examination of the association of monsoon precipitation with θ_{eb} in areas local to each monsoon region, and exploration of the relationship between precipitation and θ_{eb} in remote regions is left for future work.

We recognize that the covariation of θ_{eb} with monsoon precipitation may be more complicated than can be described by the simple QE framework used in previous theoretical studies. Our analyses do reveal such complexity, and the particular finding that monsoon precipitation covaries with θ_{eb} over the deserts located poleward of some monsoons motivates a preliminary investigation of the covariance of precipitation with the dry shallow circulations associated with those deserts (Thorncroft and Blackburn 1999; Thorncroft et al. 2011; Trenberth et al. 2000; Zhang et al. 2008). This study also includes a brief analysis of lead–lag relationships between monsoon precipitation and θ_{eb} in one regional monsoon. The main task of this paper though is a straightforward documentation of the contemporaneous relationship between observed monsoon precipitation and local θ_{eb}.

The next section of this paper presents the data sources and methods used for the linear regression analysis that forms the core of this work. Results of the regression analyses are presented in section 3, which also explores both the sensitivity of the results to the data source and antecedent relationships in Australia. The paper ends with a short summary and discussion. An appendix presents some details concerning methodological choices.

2. Data and methods

a. Data sources

Global distributions of θ_{eb} were calculated using subcloud temperature (T_b), subcloud specific humidity (q_b), and subcloud pressure from both the 40-yr European Centre for Medium-Range Weather Forecasts (ECMWF) Re-Analysis (ERA-40; Uppala et al. 2005) and the National Centers for Environmental Prediction–National Center for Atmospheric Research (NCEP–NCAR) reanalysis (Kalnay et al. 1996). Output for model level 57 (of 60 total levels) was used for the ERA-40 reanalysis and model level 27 (of 28) was used for the NCEP reanalysis, both of which follow the terrain about 20 hPa above the surface. For both reanalyses, θ_{eb} was calculated from monthly-mean data following Emanuel (1994), where

$$\theta_{eb} = T\left(\frac{P_o}{P_d}\right)^{R_d/(c_{pd}+c_l r_t)} (H)^{-rR_v/(c_{pd}+c_l r_t)}$$
$$\times \exp\left[\frac{L_v r}{(c_{pd}+c_l r_t)T}\right]. \quad (1)$$

The quantity T is the temperature, p_o and p_d are the reference pressure (1000 hPa) and the partial pressure of dry air, R_d and R_v are the gas constants of dry air and water vapor, c_{pd} and c_l are the heat capacities for dry air and liquid water, r and r_t are the water vapor mixing ratio and total water mixing ratio (although no condensed atmospheric water is considered here), H is relative humidity, and L_v is the latent heat of vaporization. While θ_{eb} is a nonlinear function of temperature and specific humidity and should thus be calculated from data sampled on subdaily time scales, preliminary analysis (not shown) revealed extremely similar results, for this analysis of interannual variability, using either the monthly mean of four times daily θ_{eb}, or the monthly mean of daily maximum θ_{eb} (as in Nie et al. 2010). Additionally, we recognize that θ_{eb} is not directly constrained by data in all regions and times represented in these reanalyses, but we do expect the assimilation of surface meteorological data, radiosondes, and SST to provide constraints in many regions. We are also somewhat reassured by the fact that two reanalysis datasets and two precipitation products yield qualitatively similar results in many regions and by the fact that the summer-mean structure of reanalyzed θ_{eb} in South Asia was validated against radiosonde data by Boos and Kuang (2010).

For SST, we use the National Oceanic and Atmospheric Administration (NOAA) National Climatic Data Center (NCDC) extended reconstructed sea surface temperature (ERSST2) database (Smith and Reynolds 2004). The quantity T_u and 700-hPa wind were obtained from the ERA-40 reanalysis (Uppala et al. 2005).

Time series of regional precipitation anomalies were calculated for six monsoon regions using data from both the Global Historical Climatology Network (GHCN; Peterson and Vose 1997) and the Global Precipitation Climatology Project (GPCP; Adler et al. 2003). The GPCP dataset incorporates satellite information, includes precipitation over the oceans, and is available from 1979 onward. The GHCN data are derived from rain gauges, are available from 1900 on, includes data only over land, and are available in a globally gridded format from the University of Delaware's Center for Climate Research (Matsuura and Willmott 2011).

Precipitation was averaged over six geographic areas chosen to reflect the interannual variability of regional monsoons and to generally be consistent with prior studies (Fig. 1). For instance, the West African domain (10°–20°N, 20°W–10°E) corresponds to a typical area used for indices of Sahel rainfall (Janowiak 1988). The South Asian domain (5°–27°N, 60°–100°E) combines the prominent rainfall regions of the Indian summer monsoon and the Bay of Bengal (Wang and Fan 1999). The North American monsoon domain (20°–35°N, 115°–100°W)
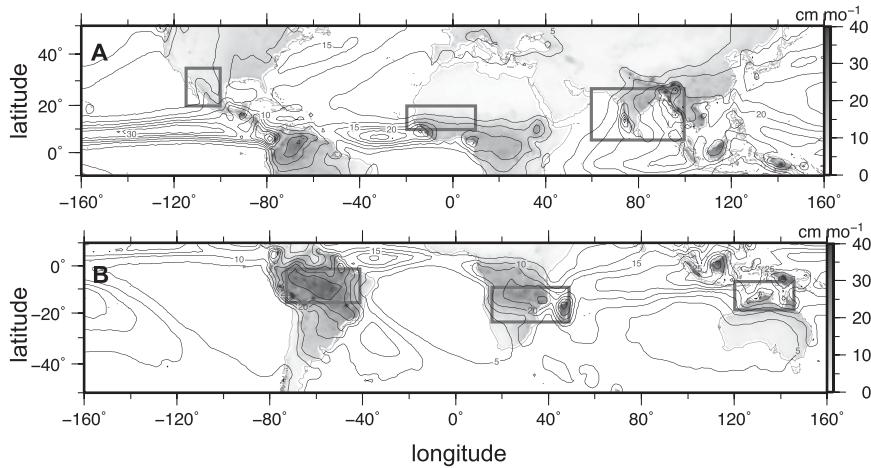
FIG. 1. Local summer-mean precipitation, (a) JJA mean with boxes drawn around the regions used to define precipitation indices in West Africa, South Asia, and North America and (b) DJF with boxes indicating precipitation index regions for Australia, East Africa, and South America. Precipitation data are GHCN (shading; cm month^{-1}) and GPCP (solid contours; contour interval of 5 cm month^{-1}).

includes the regions of Mexico and the southwestern United States dominated by early and late monsoon season precipitation (Douglas et al. 1993; Gutzler 2004). The South American monsoon domain (16°–2°S, 70°–40°W) includes the region of maximum summer precipitation over central Brazil (Gan et al. 2004) and extends both west and east across the Amazon basin, consistent with the extent of the South Atlantic convergence zone (Vera et al. 2006). The East African domain (24°–9°S, 16°–50°E), although often not identified with a classical monsoon circulation, is the site of a seasonal tropical convergence zone associated with local maxima in θ_{eb} and T_u (McHugh 2004). The Australian domain (20°–5°S, 120°–146°E) is similar to that used for numerous indices of Australian monsoon rainfall (Colman et al. 2011; Wang and Ding 2008). Some of the regions chosen for averaging precipitation include the climatological mean precipitation maximum while others are located on the periphery of that maximum. While this is not ideal, we chose to use rainfall indices similar to those in previous studies to facilitate comparison between our results and prior analysis of covariance with SST. There is qualitative agreement between the monsoon domains in Fig. 1 and the continental monsoon regions of Wang and Ding (2008).

We recognize that the dynamics responsible for precipitation may vary across these six regions and that some of them may not be considered sites of classical monsoon circulations by some investigators, but we set those issues aside for now. Nie et al. (2010) found at least some consistency with a QE view of solstitial meridional flow in all of these regions, and our goal is simply to examine the interannual variability of precipitation in a similar QE framework.

b. Analysis methods

In this study, we calculate correlation and regression coefficients for the following fields projected onto precipitation: SST, θ_{eb}, q_b, T_b, 700-hPa horizontal wind, and T_u. All the subcloud variables were evaluated on sigma levels about 20 hPa above the surface (as described above), and T_u was averaged from 200 to 400 hPa. All analyses used 3-month-averaged time series for the full calendar year, except for the analyses of auto- and cross correlations presented in section 3e, which used monthly data. The 3-month averages were taken over the standard seasonal periods of December–February (DJF), March–May, June–August (JJA), and September–November, and only minor sensitivity to the choice of these periods was found. Use of the 3-month averages reduces the signal from subseasonal variability, and use of the data for the entire year allows the influence of changes in the length of the rainy season to be included in our results. Using data for the entire year also allows possible changes in winter precipitation unrelated to summer monsoon dynamics to influence the results, but preliminary analyses (discussed in the appendix) show qualitatively similar results for full-year and local summer periods. Furthermore, since climatological monsoon onset and withdrawal dates can vary greatly between regions within the same hemisphere, use of a single "summer" period long enough to include all possible onset and withdrawal dates in each hemisphere would still allow some changes in dry season precipitation to

influence results, but this influence would be greater in some regions than in others. We therefore opted for the simpler approach of using full-year data for every region. Having results that are relevant to annual-mean precipitation rather than just its local summer component might also be seen as an advantage for some applications. Details of these methodological decisions are outlined in the appendix.

The focus of this paper is on analyses where we remove the linear variability associated with an index of ENSO. While the study of the variations of θ_{eb} related to ENSO might help in understanding the detailed mechanisms by which monsoon precipitation interacts with that climate signal, we leave that task for future work and here attempt to focus on less widely studied mechanisms that might be unrelated to ENSO. This is a simplistic approach and we acknowledge that our method does not wholly remove the ENSO signal (Compo and Sardeshmukh 2010). As a proxy for ENSO, we use the Niño-3.4 index (Climate Prediction Center 2011), which is the monthly time series of SST anomalies from 5°S to 5°N and 170° to 120°W. Variability linearly related to this index is removed using

$$Y_{i,j} = X_{i,j} - \beta_{i,j} N_{3.4}, \tag{2}$$

where $X_{i,j}$ is the original observed variable (e.g., θ_{eb}) at a particular longitude (i) and latitude (j), and $\beta_{i,j}$ is the regression coefficient of $X_{i,j}$ projected onto the Niño-3.4 index ($N_{3.4}$). Specifically, $X_{i,j}$ is the linearly detrended time series of 3-month average anomalies relative to the annual cycle. The annual cycle was obtained by averaging monthly values over all the years of the record. The quantity $Y_{i,j}$ is the variable of interest following the removal of the linear variability associated with the Niño-3.4 index, and we regress $Y_{i,j}$ onto the six regional precipitation indices, also linearly detrended, to identify spatial patterns that are linearly independent of that index.

Assessing statistical significance is complicated by the fact that the data possess spatial covariance and temporal autocorrelations. Autocorrelations of the monsoon domain precipitation indices (spatially averaged over the boxes shown in Fig. 1) generally dropped below the 95% significance level within 2 months, and autocorrelations of regionally averaged θ_{eb} dropped below this level after a few months (see discussion of correlation functions in section 3e). Brown and Bretherton (1997) found monthly values of θ_{eb} and T_u to have statistically significant autocorrelations at the 95% level for a representative time of 4 months and so reduced the number of degrees of freedom in their monthly data by a factor of 4; we take the somewhat arbitrary but even

more conservative approach of reducing our degrees of freedom by the same factor of 4 for the 3-monthly data. The decorrelation time scale for the 3-monthly averaged precipitation time series is less than one 3-month interval: within 3 months the autocorrelation function falls below the 95% confidence level. This makes the correlation coefficients significant at the 95% level for a value of 0.3 for GHCN data and 0.4 for the shorter GPCP data. We use these thresholds for correlation coefficients to delineate regions with statistically significant linear relationships.

To evaluate antecedent relationships and the persistence of precipitation and θ_{eb}, sample auto- and cross-correlation functions were computed using the method of Box et al. (1994), with the lag-zero autocorrelation normalized to unity.

3. Results

a. θ_{eb} versus precipitation

Regression coefficients for the 3-month-averaged full-year time series of ERA-40 θ_{eb} anomalies projected onto the GHCN precipitation anomalies are shown in Fig. 2 for the six monsoon regions. These results are based on data for 1958–2002, the period of the ERA-40 data, and the signal linearly related to the Niño-3.4 index was removed from θ_{eb} prior to the regression. Qualitatively similar results were obtained using the local summertime series (see the appendix for the example of West Africa).

For all six monsoon regions, positive precipitation anomalies are associated with positive continental θ_{eb} near and slightly poleward of the peak climatological precipitation. Positive regression patterns also occur over the nearby oceans for the South Asian, South American, and eastern African monsoons.

In particular, enhanced Sahel precipitation is associated with a band of enhanced θ_{eb} that stretches across Africa at about 20°N (Fig. 2a). Enhanced South Asian monsoon precipitation is linearly related to enhanced θ_{eb} over northern India and the Himalayas, which are poleward of the box used for the precipitation index, as well as with enhanced θ_{eb} within and immediately south of that box (Fig. 2b). This is more spatially extensive than the area of positive correlations seen for the other monsoon regions, and the magnitudes of the regression coefficients are consistent with an increase in the land–ocean θ_{eb} gradient during strong years of the South Asian monsoon. Precipitation in the North American monsoon is positively related to θ_{eb} over Mexico and the southwestern United States, with the positive regression pattern lying poleward of the peak precipitation even
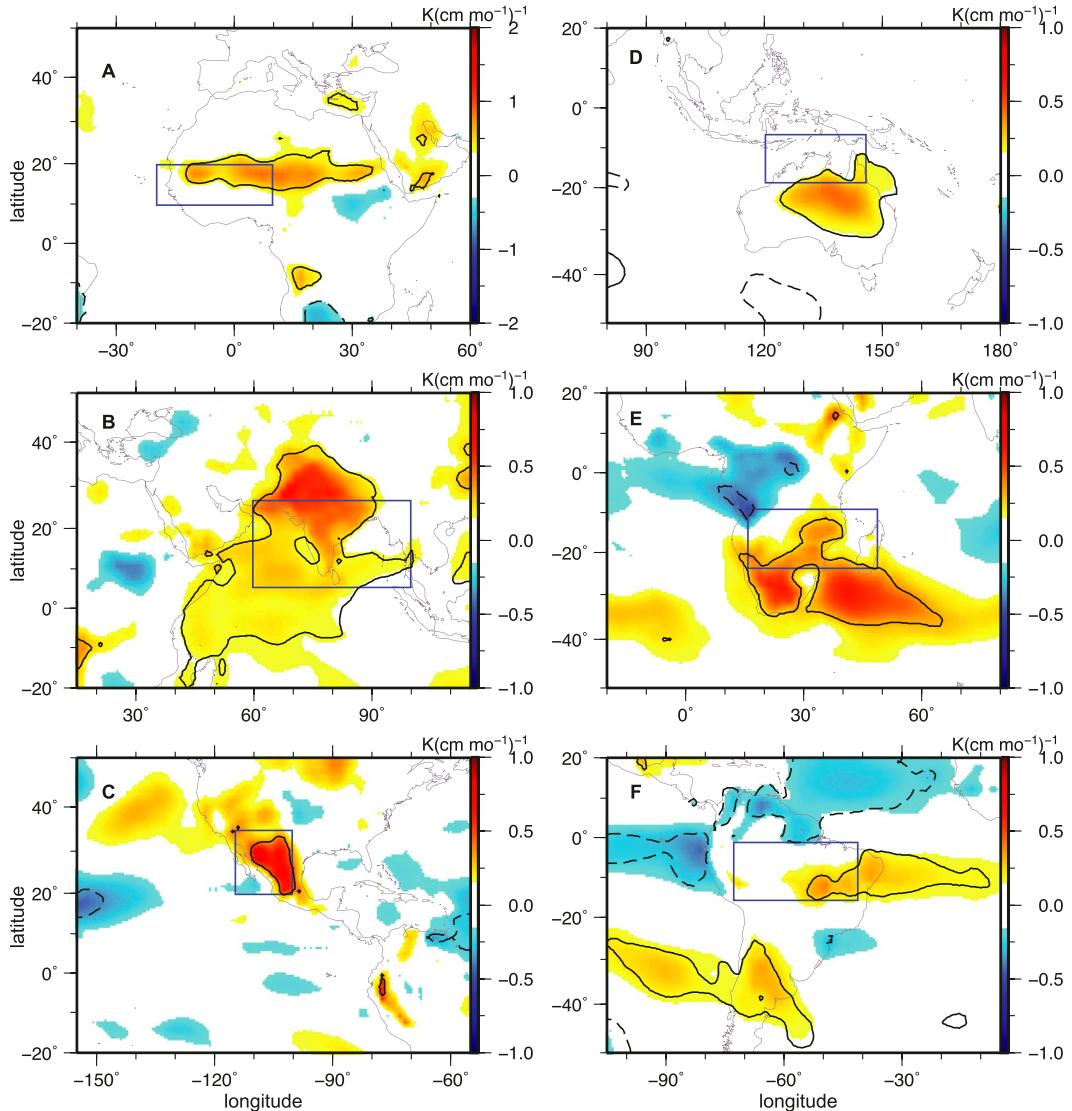
FIG. 2. Regression coefficients [shading, K (cm month^{-1})$^{-1}$] of 3-month-averaged full-year θ_{eb} (ERA-40) onto monsoon region precipitation (GHCN) for 1958–2002, following the removal of the linear variability associated with ENSO, for (a) West Africa, (b) South Asia, (c) North America, (d) Australia, (e) East Africa, and (f) South America. Precipitation was averaged over the boxed regions. Black contours (negative dashed) delineate regions where the correlation coefficient is statistically significant at the 95% confidence level. Note the different color scale for (a).

though it is located squarely within the box used to de-fine the precipitation index (Fig. 2c). Australian pre-cipitation is positively related to θ_{eb} over much of the Australian continent (Fig. 2d). Enhanced East African precipitation is associated with a band of positive θ_{eb} anomalies stretching from southern Africa to the south-western Indian Ocean (Fig. 2e). South American mon-soon precipitation is positively related to θ_{eb} in two regions: one on the eastern and poleward edge of the monsoon domain and extending over the Atlantic Ocean and one poleward of the Amazon basin over Argentina. South American precipitation is also negatively related to

θ_{eb} in the equatorial eastern Pacific and the northern tropical Atlantic (Fig. 2f).

We now present an alternate analysis of the same data, regressing limited zonal means of ERA-40 θ_{eb} onto the various GHCN monsoon precipitation in-dices, with the zonal means taken over the same lon-gitude range used for averaging precipitation. This allows for the results to be interpreted in a single spatial dimension. Figure 3 shows the summer-mean (JJA and DJF) climatology of θ_{eb} as dashed lines and the re-gression coefficients, scaled by a factor of 5 cm month^{-1} (10 cm month^{-1} for Australia) and added to the θ_{eb}
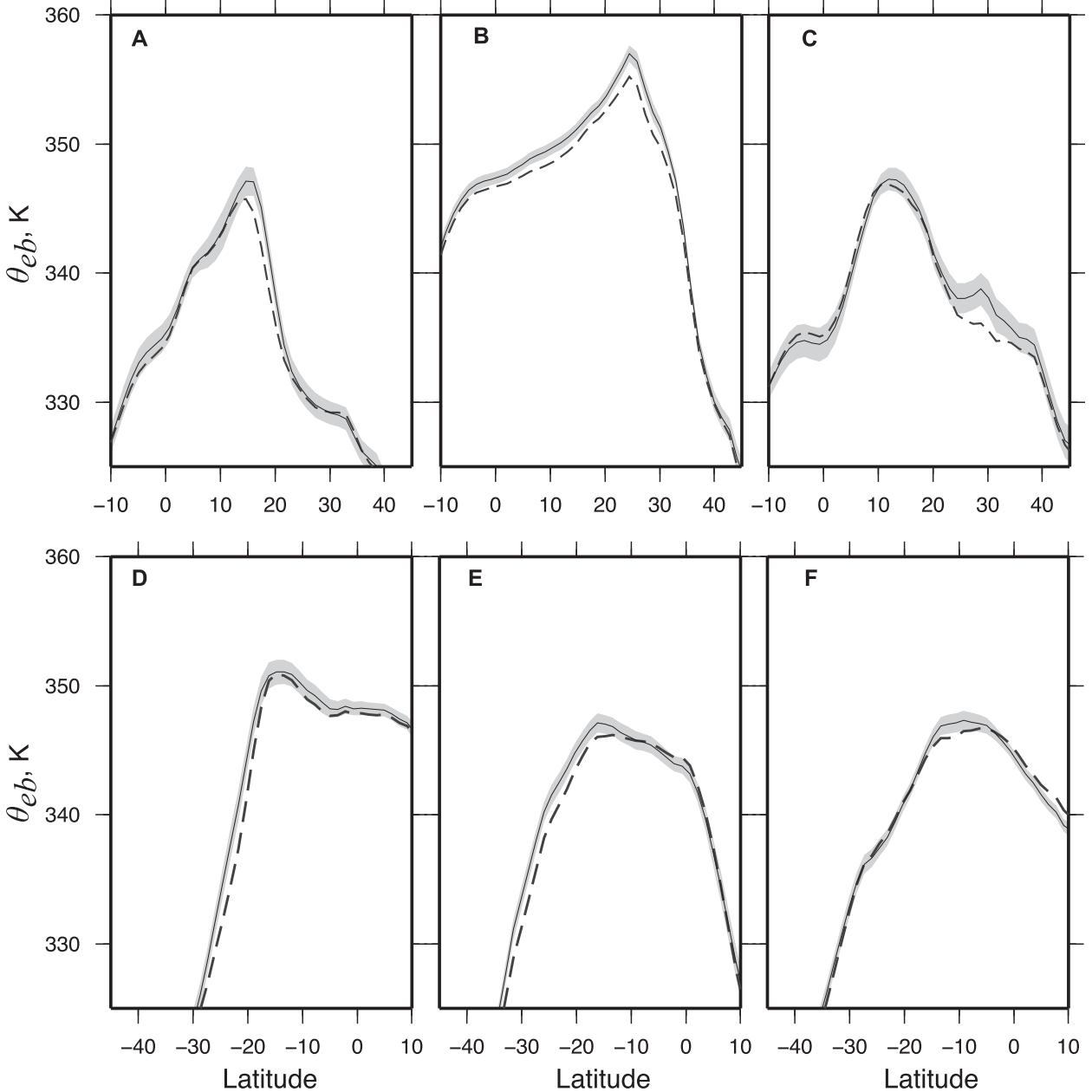
FIG. 3. Dashed lines show limited zonal means of local summer (JJA and DJF) mean ERA-40 θ_{eb}. Solid lines show θ_{eb} during a year of high precipitation, constructed by adding the summer-mean θ_{eb} to the regression coefficient scaled by a precipitation anomaly of 5 cm month^{-1} (10 cm month^{-1} for Australia). Gray shading indicates the 95% confidence interval. Regression coefficients were calculated using GHCN precipitation and limited zonal means of θ_{eb}. Results for (a) West Africa, (b) South Asia, (c) North America, (d) Australia, (e) East Africa, and (f) South America. Limited zonal means were computed across the longitudes of the boxes in Fig. 2.

climatology, as solid lines. The gray envelopes around the solid lines indicate the 95% confidence intervals associated with the scaled regression coefficients. The scaling factors correspond approximately to the maximum amplitude of the precipitation anomalies, so that the solid lines represent θ_{eb} during wet monsoon years. For the South Asian monsoon, the θ_{eb} maximum simply

increases in amplitude (Fig. 3b) during wet years, consistent with the hypothesis of Eltahir and Gong (1996). For the West African monsoon, the θ_{eb} maximum increases in amplitude and shifts poleward (Fig. 3a). A pattern common for all of the monsoon domains (except South Asia) is an increase of θ_{eb} confined to regions poleward of the summer θ_{eb} maxima (Figs. 3a,c–f),

which is distinct from the previously proposed idea that the meridional gradient of θ_{eb} increases equatorward of the summer maximum during wet years (Eltahir and Gong 1996). Although the meridional gradient of θ_{eb} in the summer climatology is strong compared to the change in θ_{eb} between wet and dry years, the increase in θ_{eb} poleward of the summer maxima is statistically significant, is seen in five of the six monsoon regions, and in some regions extends well into the subtropics. South Asia also shows an increase in θ_{eb} poleward of the climatological θ_{eb} maximum during wet years, but unlike in the other regions this is part of a simple increase in the amplitude of the climatological maximum.

For all six regions, the regression patterns extend beyond the region within which the precipitation index was defined. However, the regression coefficients in areas remote from the monsoon regions (i.e., outside the regions shown in Figs. 2–7) were not statistically significant in some combinations of datasets examined in this study. For this reason, we focus here on the regression patterns local to the monsoon regions and leave the examination of the remote patterns, their sensitivity to data product, and their field significance for future work.

Although we further discuss possible mechanisms underlying the regression patterns in a later part of this paper, we note here that even a local positive relationship between θ_{eb} and precipitation is nontrivial because θ_{eb} is a conserved variable: θ_{eb} would not change if precipitation simply cooled and moistened low-level air without altering its specific entropy. A strong positive relationship between column water vapor and precipitation has been the subject of much investigation (e.g., Bretherton et al. 2004), but those studies have been largely limited to oceanic regions and cannot easily explain the nature of continental patterns presented here.

b. Sensitivity to datasets

Analyses presented thus far used the globally gridded GHCN dataset, which is based on continental rain gauge information. To test the sensitivity of our results to the data source, we also use the GPCP precipitation product, which has global coverage and is based on both satellite and rain gauge data. Regression analyses of θ_{eb}, still calculated from the ERA-40 data, projected onto GPCP monsoon precipitation are presented in Fig. 4. These analyses used data from 1979 to 2002 (compared with 1958–2002 for Fig. 2), as the GPCP data begin in 1979 and the ERA-40 data ends at 2002.

The patterns of regression coefficients for the GPCP data are similar to those for the GHCN data in that most GPCP precipitation indices show a positive relationship with θ_{eb} near and just poleward of the peak

summer-mean precipitation. However, there are notable differences between the GHCN and GPCP patterns. The size of the statistically significant region has decreased for South Asia, and the largest regression coefficients are located closer to the equator (over southern India) in the GPCP data. Both the GPCP and GHCN regressions show a positive relationship between Sahel rainfall and θ_{eb} over large parts of northern Africa, but the region of positive regression coefficients is located farther east, extends farther north, and has higher peak amplitudes for the GPCP data. The statistically significant region has become almost vanishingly small in South America for the GPCP data, and the region of positive regression coefficients for East Africa has decreased greatly in size and is no longer located poleward of the mean precipitation peak. The patterns of ERA-40 θ_{eb} regressed onto the GHCN precipitation for 1979–2002 (not shown) have more in common with Fig. 4 than with Fig. 2, while patterns for the earlier period 1958–78 (also not shown) have more in common with Fig. 2 than with Fig. 4. These results suggest that the differences between Figs. 2 and 4 may reflect differences in the interannual variability between the two time periods. The GPCP precipitation includes data over the oceans, whereas the GHCN is limited to land, and this may also account for the differences between Figs. 2 and 4.

To test the sensitivity of our results to the choice of reanalysis product, we also calculated θ_{eb} from the NCEP reanalysis (Fig. 5). As with the ERA-40 results in Fig. 4, we regress the NCEP θ_{eb} onto the GPCP precipitation indices for 1979–2002. While there are differences in the amplitude and spatial extent of the extrema, the patterns are quite similar to those obtained using ERA-40. In particular, most regions (but not South America or East Africa) show a positive relationship between precipitation and θ_{eb} local to and immediately poleward of the mean precipitation peak.

c. The quantities q_b, T_b, and T_u versus precipitation

While variations of θ_{eb} are of interest in their own right, it may be useful to know whether changes in humidity or temperature make a dominant contribution to the relationship between θ_{eb} and precipitation. The positive relationship between precipitation and θ_{eb} local to and slightly poleward of the index region is mostly due to the relationship between q_b and precipitation (Fig. 6). In contrast, the regression patterns between T_b and the monsoon region precipitation are, at least over continents, opposite in sign to those for θ_{eb} (Fig. 7). Over the oceans the relationship between T_b and precipitation typically has the same sign as that between θ_{eb} and precipitation. For instance, the region of high θ_{eb} over the southern Indian Ocean that is associated with
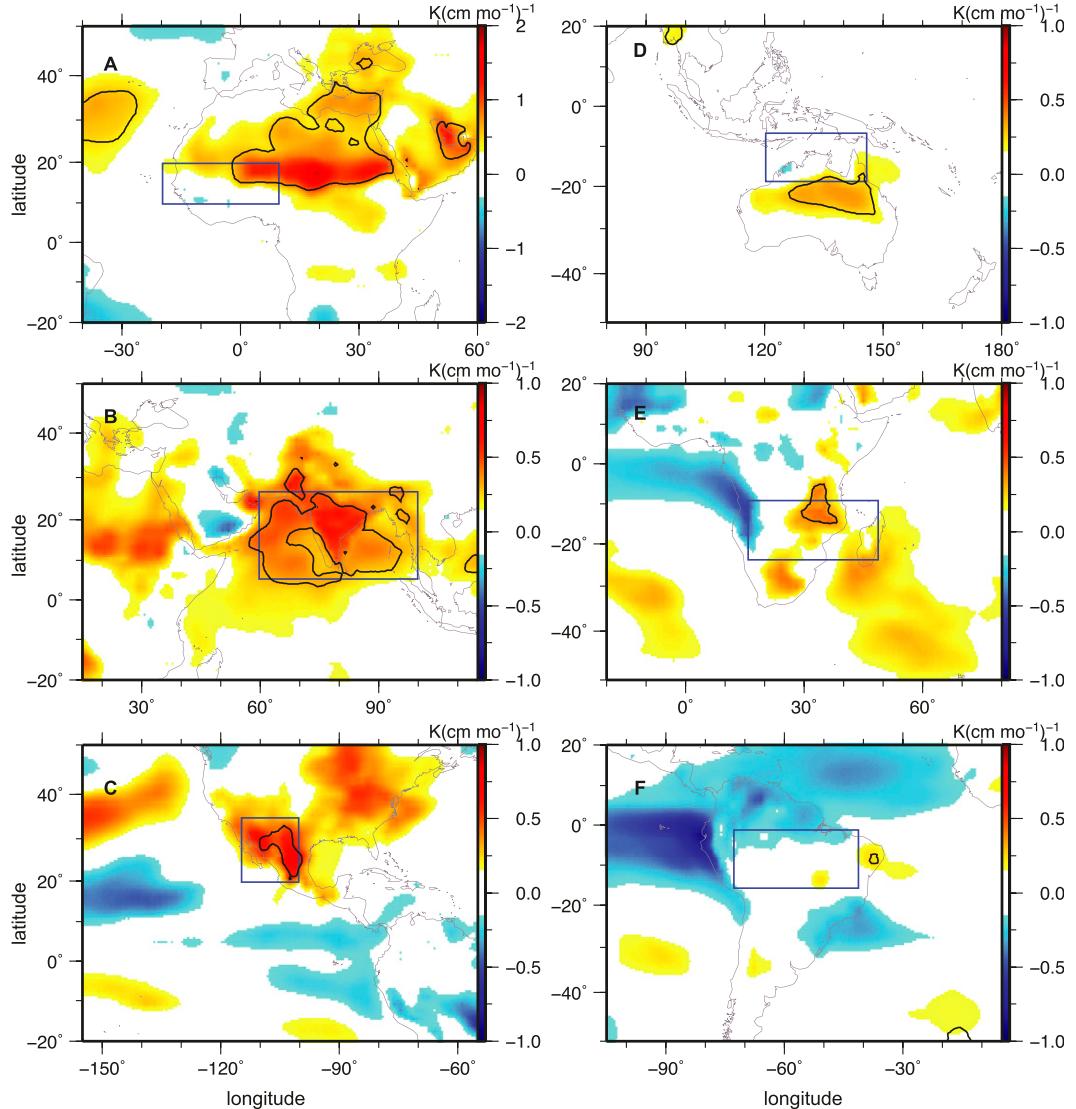
FIG. 4. As in Fig. 2, but for regression of ERA-40 θ_{eb} onto GPCP monsoon region precipitation for 1979–2002, with regression coefficients (shading) in units of K (cm month^{-1})$^{-1}$.

enhanced East African precipitation has the same sign for regressions of θ_{eb}, q_b, and T_b, but the regression coefficient over continental Africa is negative for T_b and positive for both θ_{eb} and q_b. This is consistent with a simple scenario in which the oceanic patterns result from SST changes that control the thermodynamic state of the subcloud layer without changes in subcloud relative humidity or air–sea temperature difference. Explaining these patterns over land is less straightforward, because while one does expect precipitation over land to be accompanied by enhanced specific humidity and reduced surface air temperature (Eltahir 1998; Trenberth and Shea 2005), changes in θ_{eb} signify a net change in the entropy of the subcloud layer rather than just its

partitioning between sensible and latent components. Eltahir (1998) hypothesized that soil moisture could take part in a local positive feedback on precipitation by enhancing the subcloud energy content through reductions in both surface albedo and surface longwave emissions. The local positive relationships between θ_{eb} and precipitation seen here are consistent with that hypothesis, although interactions with large-scale dynamics may also operate. Further investigation would be necessary to establish the influence that soil moisture has on θ_{eb} and to distinguish it from other influences such as large-scale advection of θ_{eb} or other controls on surface fluxes.

The statistically significant patterns for q_b and T_b regressed on South Asian precipitation are less spatially
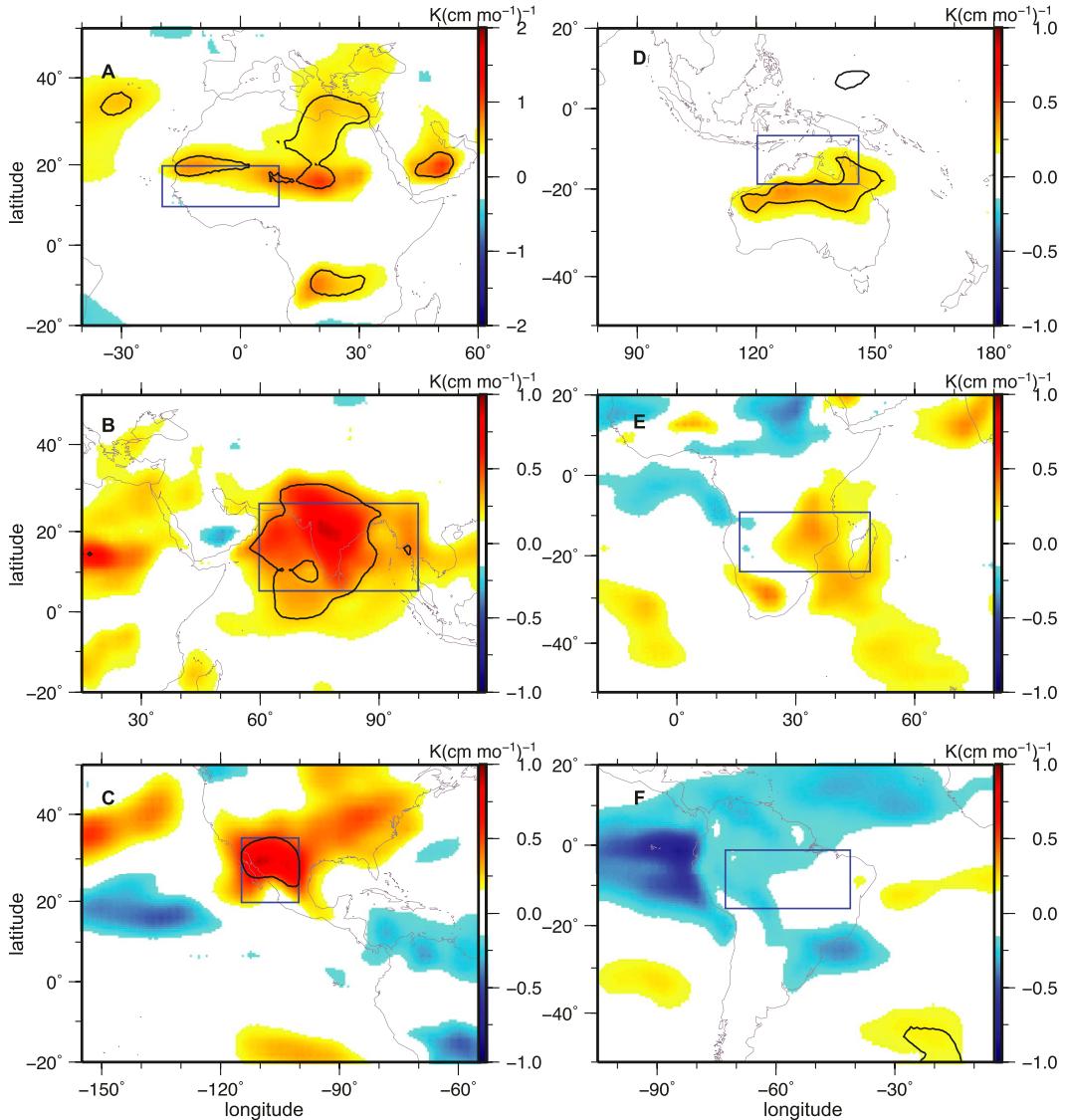
FIG. 5. As in Fig. 2, but for regression of NCEP θ_{eb} onto GPCP monsoon region precipitation for 1979–2002, with regression coefficients (shading) in units of K (cm month^{-1})$^{-1}$.

extensive than the regression patterns for θ_{eb}. This results from the nonlinear dependence of θ_{eb} on q_b (see the appendix) and illustrates the power of using θ_{eb} instead of surface air temperature or humidity to interpret variations in monsoon strength.

Also plotted in Fig. 6 (as green contours) are correlation coefficients between precipitation and T_u. Consistent with a QE framework, maxima of θ_{eb} and T_u are spatially coincident in many of Earth's regional summer monsoons (Nie et al. 2010), so one might expect interannual variations of those quantities to have similar patterns if QE holds. Indeed, T_u does seem to covary with precipitation in a somewhat similar fashion to θ_{eb} in some regions. The correlations between monsoon

precipitation and T_u are neither as pronounced as, nor exactly collocated with, the peak correlations between precipitation and θ_{eb}. However, there are similarities worth noting. For example, positive correlations are seen between Australian precipitation and T_u over central Australia. The positive correlation of Sahel precipitation with T_u over the eastern Atlantic and Mediterranean Sea is located well poleward of the peak θ_{eb} signal and only has small regions that exceed the statistically significant threshold of 0.3. Nevertheless, the relationships of Sahel precipitation with T_u, θ_{eb}, and q_b may be consistent with the idea that positive anomalies of Mediterranean SST produce enhanced Sahel rainfall through the advection of moisture across the Sahara
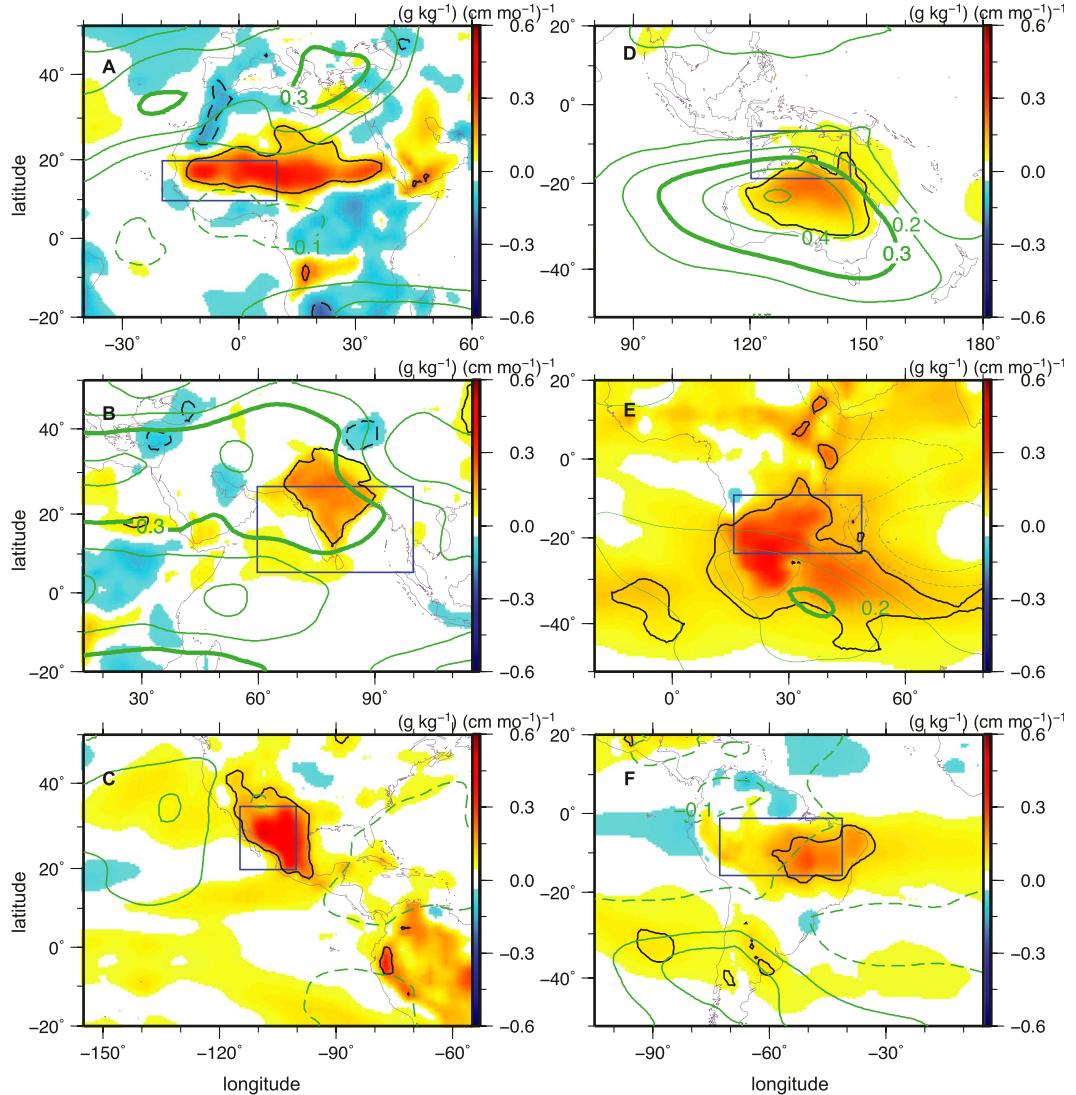
FIG. 6. Regression coefficients [shading; $\mathrm{g\,kg^{-1}\,(cm\,month^{-1})^{-1}}$] of 3-month-averaged full-year q_b (ERA-40) onto monsoon region precipitation (GHCN), for 1958–2002, following removal of the linear variability associated with ENSO, for (a) West Africa, (b) South Asia, (c) North America, (d) Australia, (e) East Africa, and (f) South America. Green contours (0.10 contour interval; 0 contour not shown) are correlation coefficients between precipitation (GHCN) and upper troposphere temperatures (T_u, ERA-40; 200–400 hPa); dashed contours indicate negative correlations (values are significant at values above or below +0.3 or −0.3, bold contour). Precipitation was averaged over the boxed regions. Black contours delineate regions where the correlation coefficient between q_b and precipitation is statistically significant at the 95% confidence level.

(Rowell 2003). No strong local correlation between precipitation and T_u is seen in the Americas.

It is intriguing that the positive correlations between precipitation and T_u in several regions have an equatorial minimum, with maxima in either hemisphere roughly equidistant from the equator. This meridional structure, symmetric about the equator, is seen for the Sahel, South Asia, and Australia (Figs. 6a,b,d, respectively), though the winter hemisphere maxima lie outside of the areas plotted in Fig. 6 and are not shown here. This type of

temperature structure is consistent with an angular momentum-conserving Hadley circulation that has an off-equatorial ascent branch (Lindzen and Hou 1988) and can be seen in simple models of monsoon flow that couple θ_{eb} with T_u in a QE framework (e.g., Emanuel 1995 and Boos and Emanuel 2008b). Excitation of $n = 1$ equatorial Rossby waves might also produce equatorially symmetric anomalies through entirely linear dynamics (Matsuno 1966). Both Gill (1980) and Rodwell and Hoskins (1996) show a stationary response both
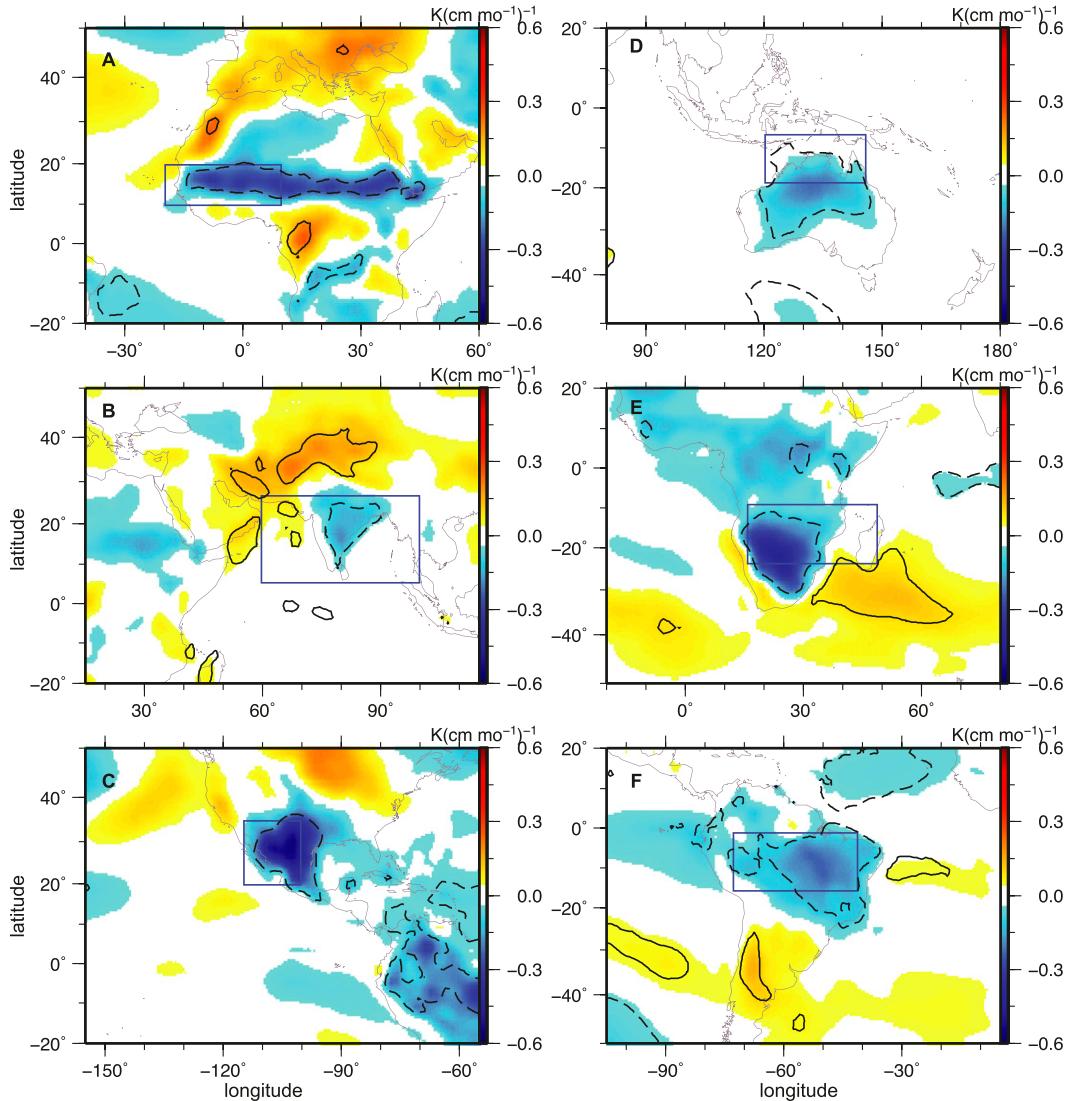
FIG. 7. As in Fig. 6, but for T_b [shading, K (cm month^{-1})$^{-1}$].

north and south of the equator, at locations west of the idealized off-equatorial steady heating.

d. Wind versus precipitation

While a thorough study of the covariation of precipitation with large-scale winds is beyond the scope of this manuscript, we do examine correlations between precipitation and flow in the lower free troposphere. This is motivated by the relatively recent finding that interannual variations of Sahel precipitation in climate models is related to the strength of the Sahara low (Biasutti et al. 2009; Haarsma et al. 2005; Thorncroft et al. 2011) and by the identification of shallow circulations in the seasonal-mean climatologies of summer meridional flow in Australia and southern Africa (e.g.,

Nie et al. 2010). These shallow circulations consist of the near-surface poleward flow that extends beyond the primary monsoon precipitation maximum and terminates near the peak subcloud potential temperature maximum (θ_b, not θ_{eb}). Since the positive anomalies of θ_{eb} and q_b that are associated with enhanced monsoon precipitation also extend poleward of the main precipitation maximum into the desert regions of Australia and West Africa, it seems reasonable to ask if they are associated with some change in the shallow flow. A working hypothesis is that the advection of dry air by the shallow circulation into the primary monsoon convection zone reduces the rate of monsoon precipitation. This is consistent with discussion of the possible influence of shallow flow in the Sahara low on the seasonal
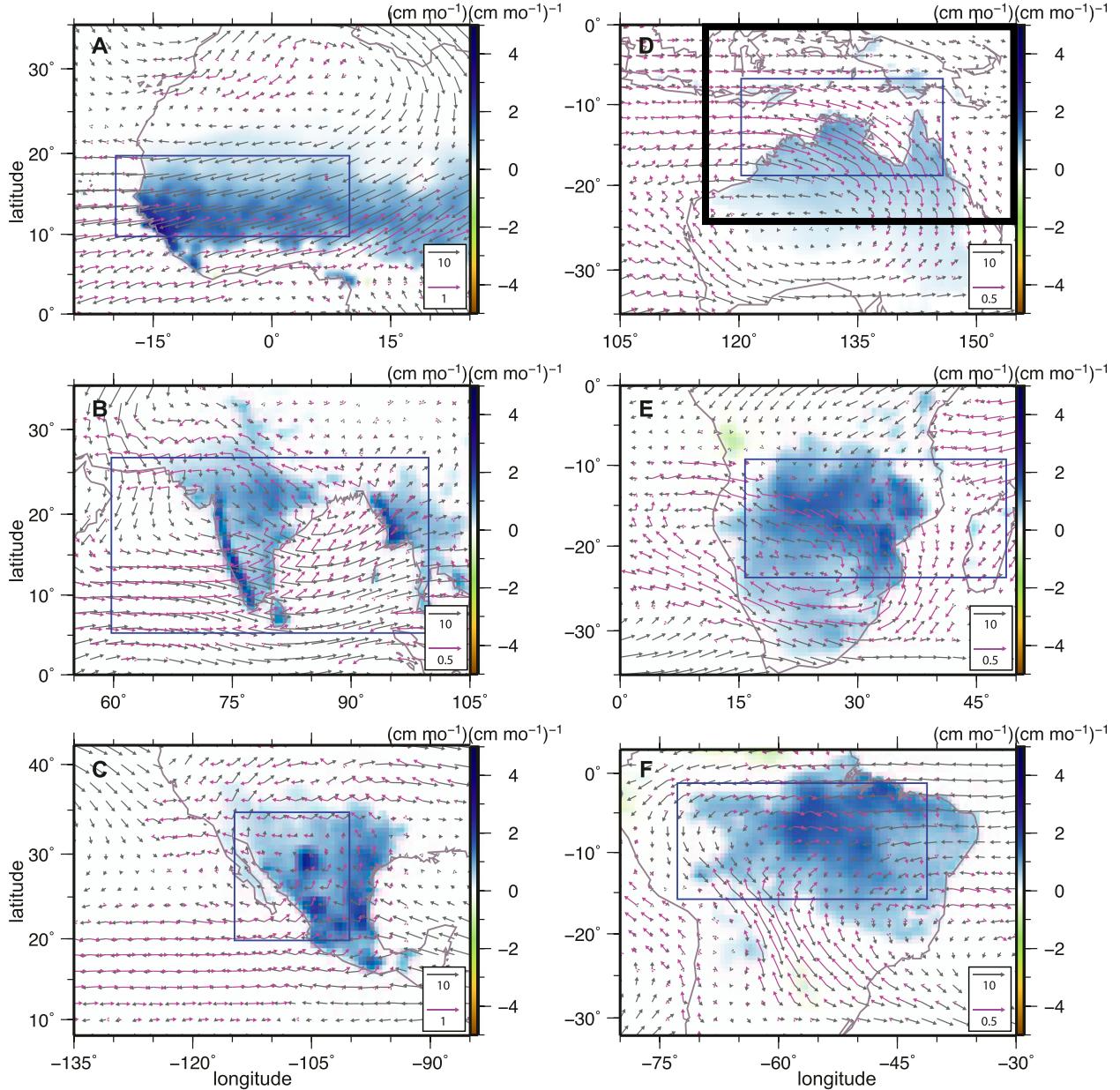
FIG. 8. Regression coefficients [shading, cm month^{-1} (cm month^{-1})$^{-1}$] of 3-month-averaged full-year precipitation (GHCN) onto monsoon region precipitation for 1958–2002, following removal of the linear variability associated with ENSO, for (a) West Africa, (b) South Asia, (c) North America, (d) Australia, (e) East Africa, and (f) South America. Vectors are horizontal winds at 700 hPa. Gray vectors are the local summer climatological winds (m s^{-1}) and magenta vectors are the coefficients [m s^{-1} (cm month^{-1})$^{-1}$] of winds regressed onto precipitation. Reference vectors (inset boxes) are scaled to the value indicated in units of m s^{-1} for the gray vectors and units of m s^{-1} (cm month^{-1})$^{-1}$ for the magenta vectors. Regression shading and vectors are plotted only where the regression of precipitation onto the precipitation index or either the zonal or meridional wind onto the precipitation index is statistically significant at the 95% confidence level. Precipitation was averaged over the boxed regions.

cycle of Sahel precipitation by Zhang et al. (2008); Peyrillé and Lafore (2007) present some relevant numerical model results.

Figure 8 presents regressions of both the full precipitation field (shading) and the 700-hPa horizontal wind (magenta vectors) projected onto the monsoon domain precipitation indices. Also plotted, for comparison, is the summer-mean (JJA and DJF) 700-hPa horizontal wind (gray vectors). The 700-hPa level is above or near the top of the low-level poleward branch

of the deep baroclinic monsoon flow and is within the upper equatorward branch of the shallow flow (which projects strongly onto a second baroclinic mode). Thus, for those monsoons with a pronounced shallow meridional circulation, such as West Africa and Australia, the 700-hPa mean summer flow is directed toward the equator in the region of the precipitation maximum. This equatorward flow is part of a broader 700-hPa anticyclone centered over the desert regions. Equatorward flow is also seen in the southwest part of the box over which precipitation was averaged in East Africa and northwest of India in an intense heat low (Ramage 1966).

Regression analysis shows that enhanced precipitation is associated with enhanced poleward flow at 700 hPa in most regions (especially in Australia, the Sahel, and East Africa), which could alternatively be viewed as a weakening of the climatological equatorward flow at that level. This weakening of the 700-hPa flow could be due to a weakening of the dry shallow circulation or a vertical expansion of that circulation. It could also be due to a vertical expansion of the lower poleward branch of the deep baroclinic circulation or a strengthening of that first baroclinic part of the flow, but such first baroclinic changes would not be expected to produce the 700-hPa cyclones centered over the deserts that are seen in the regression patterns (e.g., Figs. 8d,e). Both Haarsma et al. (2005) and Biasutti et al. (2009) found that enhanced Sahel precipitation was associated with negative anomalies of sea level pressure and 925-hPa geopotential height in the Sahara. This is inconsistent with a generic weakening of the shallow heat low circulation during times of enhanced rainfall and indicates that further investigation of the relevant dynamics is needed. The fact that subcloud temperatures over continental Australia are negatively correlated with Australian precipitation (Fig. 7d) would also seem inconsistent with a strengthening of the Australian heat low during times of enhanced monsoon precipitation. We plan to more thoroughly examine interannual variations in the intensity and vertical structure of shallow flow over both Australia and northern Africa in future work.

Even in regions without a well-defined shallow circulation, the change in 700-hPa flow during wet years is clearly distinct from a simple strengthening of the climatological mean flow at that level. For example, the regression vectors are roughly perpendicular to the mean flow vectors within the eastern half of the box used to define the precipitation index in South Asia, indicating an association between positive precipitation anomalies and enhanced poleward flow at 700 hPa. In North America, enhanced monsoon precipitation is associated with anomalous southwesterly monsoon flow

from the Pacific, in contrast to the mean flow from the Gulf of Mexico. In South America, enhanced monsoon precipitation corresponds, along the poleward edge of the monsoon domain, to a reduction in the strength of the northerly low-level jet at 700 hPa. This is consistent with the results of Garreaud and Wallace (1998), where they show the development of cold fronts and convection when cold and dry midlatitude air is advected into subtropical South America. These results also show that enhanced precipitation does not simply result from enhanced low-level moisture in the absence of circulation changes.

Regardless of the reasons for these changes in the 700-hPa flow, they are consistent with the hypothesis that stronger shallow circulations inhibit monsoon precipitation by advecting low θ_{eb} (i.e., dry) air into the monsoon domain at low levels. This might be seen as a variation of the "ventilation" mechanism of Chou et al. (2001) and Chou and Neelin (2003) in which advection of low moist static energy air limited the poleward extent of a monsoon but via a shallow circulation not represented in those models. The enhancement of θ_{eb} poleward of the primary precipitation maximum also seems consistent with the application of a ventilation mechanism to interannual variability, but our analyses do not determine the relative importance of variations in the strength of a shallow circulation and the variations in θ_{eb} (which may interact with the precipitation maxima entirely through deep first baroclinic dynamics).

e. Antecedent relationships

To explore lead–lag relationships, we completed the correlation function analyses for the Australian region using the precipitation index and a θ_{eb} index computed for a region that includes continental Australia ($0°–42°S$, $120°–150°E$). Correlation function estimates (Fig. 9) show that the autocorrelations of precipitation are significant only out to 1 month of lead time, and autocorrelations of θ_{eb} are significant for about 2 months. In contrast, correlations between θ_{eb} and precipitation are statistically significant, albeit weak, when θ_{eb} leads precipitation by 5 months, and the fact that cross correlations at these lead times are greater than either of the autocorrelations is suggestive of an antecedent relationship due to more than simple persistence. The cross-correlation function falls rapidly below the significance threshold when precipitation leads θ_{eb}. When precipitation lags by 1–5 months (left of the origin), the precipitation–θ_{eb} relationship is significant at the 95% confidence level and only slightly weaker than the precipitation–ENSO correlation. At zero-lag, the precipitation–θ_{eb} relationship is at least as strong as the precipitation–ENSO relationship.
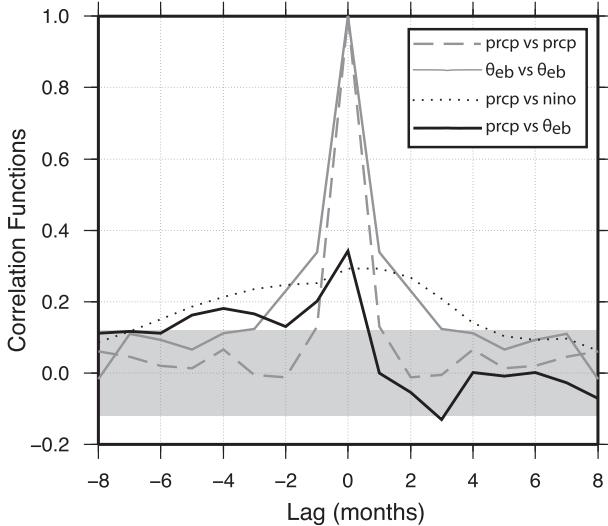
FIG. 9. Australian monsoon auto- and cross-correlation functions for 1979–2002. GPCP precipitation was averaged over 5°–20°S, 120°–146°E and ERA-40 θ_{eb} was averaged over 0°–42°S, 120°–150°E. Autocorrelations are for precipitation (dashed gray line) and θ_{eb} (solid gray line). Cross correlations are for precipitation vs θ_{eb} (solid black line) and precipitation vs the Niño-3.4 index (dotted gray line). Negative lag indicates that θ_{eb} or the Niño-3.4 index leads precipitation. Horizontal gray bar indicates correlation values that are insignificant at the 95% confidence level.

4. Conclusions

We have examined the covariation of seasonal precipitation anomalies in six monsoon regions with local θ_{eb} and several related variables. We chose to remove the variability linearly associated with the Niño-3.4 SST index in order to reduce the likelihood that our results will simply provide another perspective on the well-known association between ENSO and monsoon precipitation. We found positive precipitation in each region to be associated with enhanced θ_{eb} local to and slightly poleward of the primary monsoon precipitation maximum. This general local result held for both of the reanalysis products used to calculate θ_{eb}. The continental variations in θ_{eb} local to the precipitation maxima are mostly due to variations in q_b, with local changes in T_b having an opposite sign. The quantity T_u was also shown to covary with θ_{eb} and precipitation in ways qualitatively consistent with a strict QE hypothesis in a few regions: during times of enhanced monsoon precipitation, regions of enhanced T_u are located over the regions of enhanced θ_{eb} slightly poleward of the peak monsoon ascent zone in Australia and South Asia, with weak signals in western and eastern Africa.

Here, we summarize three distinct ways in which boundary layer moist entropy may covary with monsoon precipitation, two of which are previously recognized

relationships and a third that is relevant to the results presented in this study. For the South Asian monsoon, the climatological θ_{eb} peak simply increases in amplitude during years of enhanced precipitation. This is illustrated schematically in Fig. 10a, can also be seen in Fig. 3b, and is consistent with simple theoretical ideas for how monsoon strength relates to the amplitude of an off-equatorial θ_{eb} maximum (e.g., Emanuel 1995; Prive and Plumb 2007b). Eltahir and Gong (1996) argued that for West Africa during wet years, the meridional gradient of boundary layer moist entropy may increase due to a reduction in boundary layer moist entropy on the winter side of the equator, as shown schematically in Fig. 10b. Thus, Figs. 10a and 10b in the schematic of Fig. 10 depict previously recognized relationships by which monsoon precipitation is enhanced when the meridional gradient of θ_{eb} increases between the θ_{eb} peak and the winter hemisphere. We recognize here an additional relation between monsoon precipitation and θ_{eb}, whereby wet monsoon years are associated with enhanced θ_{eb} poleward of the climatological θ_{eb} maxima (see schematic in Fig. 10c and also Figs. 3a,c–f).

While most theoretical studies of monsoon dynamics that used a QE framework employ only a single baroclinic mode (e.g., Emanuel 1995; Chou et al. 2001), recent work has suggested that dry shallow circulations with low-level temperature maxima poleward of the region of peak monsoon precipitation may play a role in the mean state and interannual variability of monsoons (e.g., Haarsma et al. 2005; Nie et al. 2010; Biasutti et al. 2009). Our results show that the low-level moisture anomalies associated with variations in monsoon precipitation may extend into the desert regions that serve as thermal maxima for these shallow circulations and that the climatological equatorward flow at 700 hPa weakens during seasons of enhanced monsoon precipitation. This is illustrated schematically in Fig. 11, though we emphasize that it is unclear whether the increase in precipitation is due to a weakening or deepening of the shallow circulation or an increase in its moisture content. In any case, moist convection has been shown to be sensitive to the presence of dry air in the lower free troposphere (Derbyshire et al. 2004; Raymond and Zeng 2000; Tompkins 2001), and these findings suggest a particular application of this idea to interannual monsoon variability. An alternate possibility is that the desert regions and their associated shallow circulations are being modulated by Rossby waves emitted by deep cumulus convection (Bollasina and Nigam 2011; Rodwell and Hoskins 1996), with the crucial dynamics involving only deep first baroclinic motions. Regardless of the mechanism, our results emphasize the potential importance of low-level moisture anomalies poleward of the
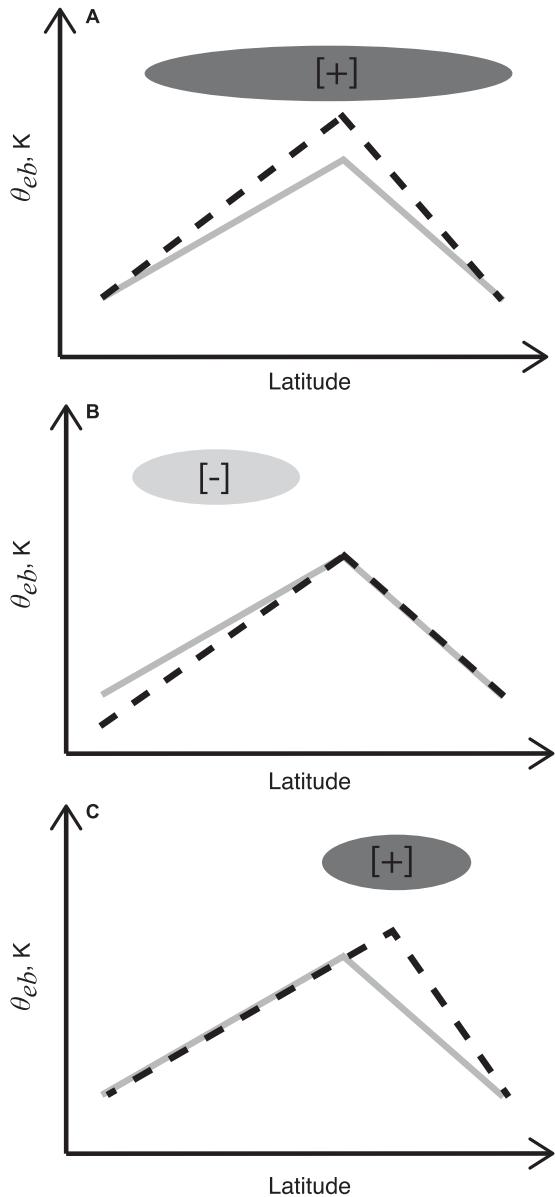
FIG. 10. Schematic of ways in which monsoon precipitation co-varies with θ_{eb}. Solid gray lines represent the basic state and the dashed black line shows θ_{eb} during years of high precipitation. Gray ovals indicate latitudes where positive or negative regression patterns would occur for θ_{eb} regressed on precipitation indices. (a),(b) The meridional gradient of θ_{eb} on the equatorward side of the θ_{eb} peak increases during wet years, which were illustrated schematically by Eltahir and Gong (1996, their Figs. 9 and 13, respectively). (c) An increase of θ_{eb} poleward of the basic state θ_{eb} maximum, with negligible change at the location of the basic state maximum.

FIG. 11. Schematic of the relationships seen in our regression analyses, for years of (a) normal precipitation and (b) high pre-cipitation. Diagrams depict the shallow meridional circulation (dashed black overturning cell) associated with a desert heat low, the deep monsoon circulation (solid gray overturning cell), and the θ_{eb} profile [dashed black line is for a wet year and solid gray line is for the basic state, repeated in (b) for reference]. A poleward contraction of the desert during wet years is included in (b), based only on speculation.

precipitation peak for the interannual variability of monsoons.

The covariation of deserts with monsoon precipitation might be evidence for a variation on the hypothesis of Charney (1975),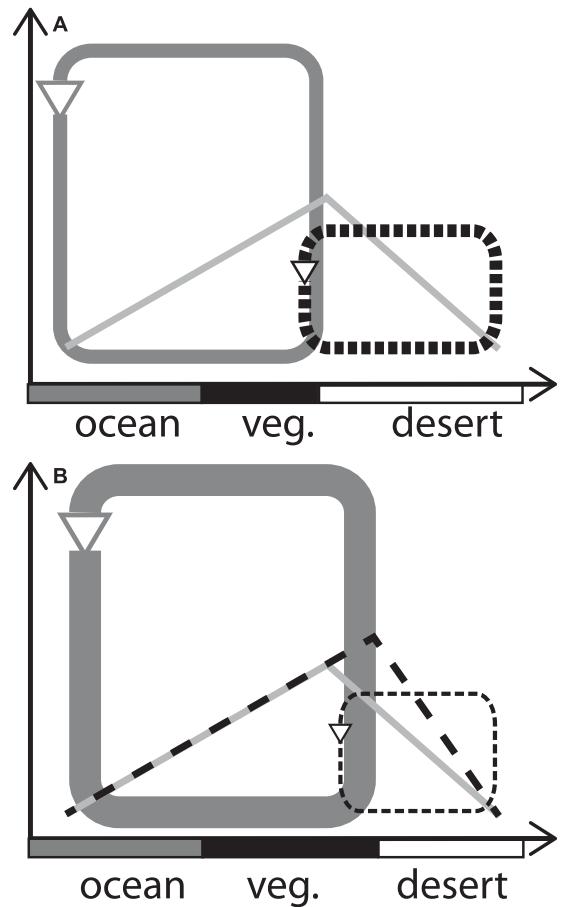 in which monsoon precipitation interacts with the surface albedo of an adjacent desert. The posi-tive anomalies of θ_{eb} over deserts seen in our analyses could be caused by negative anomalies of land surface albedo, which in turn could result from changes in the latitude of the vegetation–desert boundary or simply from the darkening of wet soil. A shift in the latitude of the desert boundary is included in the schematic of Fig. 11, and although the existence of such a shift is speculative, it would be consistent with the fact that precipitation anomalies extend into the equatorward edge of desert regions (Fig. 8).

The lack of a clear association between South Asian precipitation and θ_{eb} poleward of that region's clima-tological θ_{eb} maximum is consistent with the idea that the Himalayas and the Hindu Kush mountains insulate
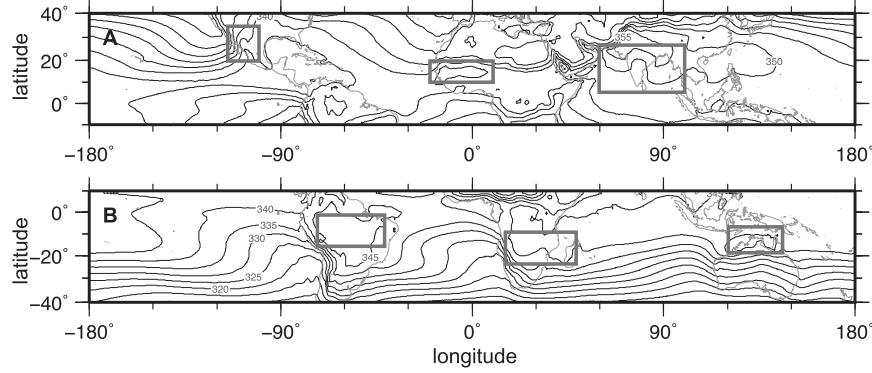
FIG. A1. (a) JJA and (b) DJF mean θ_{eb} (ERA-40; 1958–2002). Contour interval, 5 K. Boxes indicate monsoon domains used for precipitation indices.

the South Asian monsoon from the influence of nearby deserts (Boos and Kuang 2010; Boos and Hurley 2013; Chakraborty et al. 2006). If topography inhibits variations in the properties of Asian deserts from influencing the South Asian monsoon, one would expect interannual variability in that region to differ from that of monsoons that are coupled with variations in adjacent deserts.

The linear analyses presented here are only intended to be a first step in the examination of the interannual variability of observed monsoons in a QE framework. Our discussion of mechanisms was almost entirely speculative and needs to be assessed in quantitative theoretical frameworks. It is unclear whether existing QE models such as the quasi-equilibrium tropical circulation model (QTCM; Neelin and Zeng 2000) or the zonally symmetric model used by Boos and Emanuel (2008a,b) are suitable for such a task, as their dynamical structure cannot represent shallow heat low flow. It is also unclear how well dry shallow circulations are represented in more comprehensive global climate models. But regardless of theoretical progress, further examination of the observed statistics of subcloud thermodynamics may help in understanding interannual variations in monsoons.

APPENDIX

Methodological Details

In this appendix we present five figures, both for reference and to illustrate the effects of some of the methodological choices.

Summer-mean θ_{eb} climatologies are presented in Fig. A1 for comparison with the regression patterns shown in the body of this paper. These climatologies show the locations of the summer-mean θ_{eb} maxima and are consistent with those shown in Nie et al. (2010).

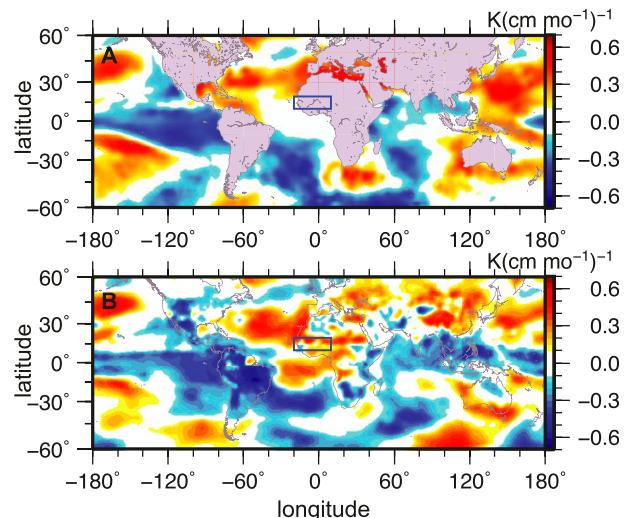Over the ocean, correlations between monsoon precipitation and SST are expected to be highly similar to

FIG. A2. Correlation coefficients for JJA, 1979–2002, for West African monsoon precipitation (GHCN) and (a) SSTs (ERSST) and (b) θ_{eb} (ERA-40). Precipitation was averaged over the boxed region.
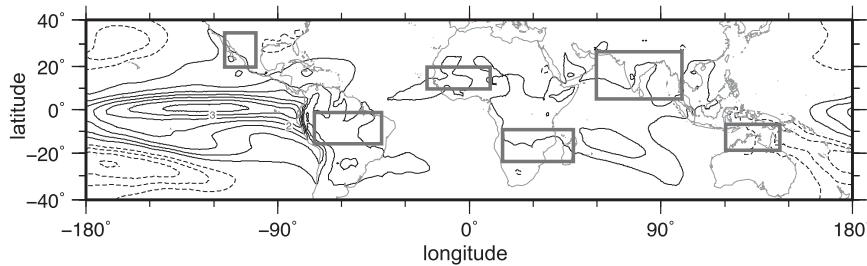
FIG. A3. Regression coefficients of 3-month-averaged full-year seasonal anomalies of θ_{eb} (ERA-40; 1958–2002) onto the Niño-3.4 index. The contour interval is $0.5\,\mathrm{K\,K^{-1}}$ and the 0 contour is not drawn; solid lines are positive, and dashed lines are negative.

correlations between precipitation and θ_{eb} if the air–sea temperature difference and subcloud relative humidity are fixed. Figure A2 shows correlations between West African precipitation and both SST and θ_{eb} and is broadly consistent with a scenario in which variations in θ_{eb} over the ocean have, at least, the same sign as variations in SST. For Fig. A2, the variability in θ_{eb} linearly associated with ENSO (which is shown in Fig. A3) has not been removed and only local summer (June–August) data were used for easier comparison with previous work. The positive signal in the North Atlantic and the negative signals in the extratropical South Atlantic and western Indian Oceans (Fig. A2) qualitatively agrees with other published correlations between the West African monsoon precipitation and SST (Caminade and Terray 2010; Lu 2009). Of course, θ_{eb} is not a function of only SST; even when a 6-month low-pass filter was used, Brown and Bretherton (1997) found a correlation coefficient of only 0.60 between SST and θ_{eb}, with variations in oceanic θ_{eb} being almost entirely due to variations in q_b. They also found that T_u was correlated more strongly with θ_{eb} than with SST, which provides strong motivation for the study of variations in θ_{eb} in general. Another obvious advantage of examining θ_{eb} is that it extends the analysis domain over land without, apparently, introducing dramatic changes to previously studied relationships in which SST was assumed to strongly control near-surface thermodynamics (e.g., Fig. A2).

Figure A4 shows the results from an analysis similar to that of Fig. A2 but with regression coefficients plotted instead of correlation coefficients and with the removal of the variability linearly associated with Niño-3.4. Patterns that are statistically significant at the 95% confidence level are outlined in thick black contours. Removal of the ENSO signal eliminates the strong statistically significant negative relationship in the eastern tropical Pacific (not shown) but leaves a strong positive relationship in the North Atlantic between precipitation and both SST and θ_{eb}. The positive relationship with θ_{eb}

extends in a zonally elongated band across the northern part of the Sahel. These sorts of relationships between precipitation and continental θ_{eb} were examined in the results section, with Fig. A4 presented here to illustrate
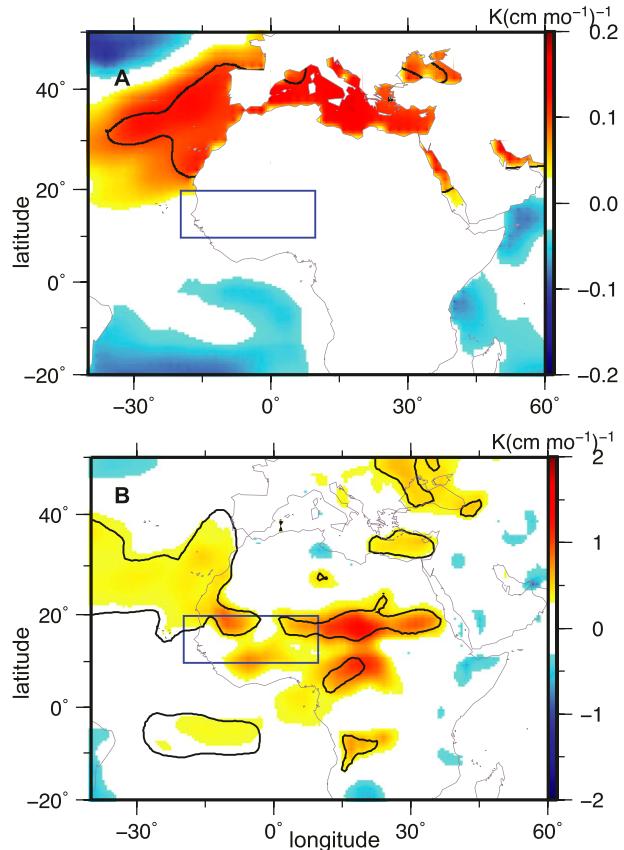

FIG. A4. Regression coefficients [shading, $\mathrm{K\,(cm\,month^{-1})^{-1}}$] for JJA, 1958–2002, for (a) SSTs (ERSST) and (b) θ_{eb} (ERA-40) onto West African monsoon precipitation (GHCN), following the removal of the linear variability associated with ENSO. Precipitation was averaged over the boxed region. Black contours delineate regions where the correlation coefficient is statistically significant at the 95% confidence level. Note the different color scales.
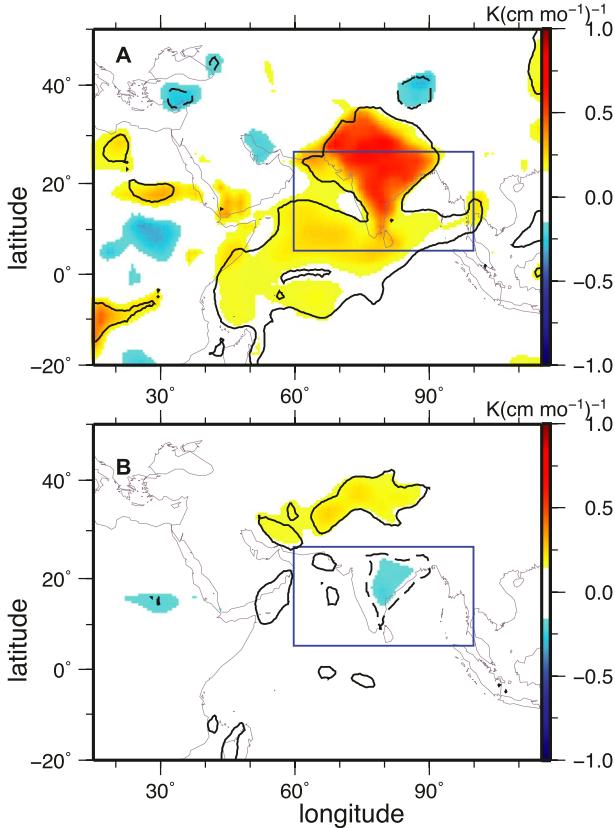
FIG. A5. Regression coefficients of modified versions of θ_{eb} (ERA-40) onto South Asian monsoon precipitation (GHCN). Color shading and black lines represent the regression coefficients $[K (cm\,month^{-1})^{-1}]$ and the 95% confidence level as in Fig. 2. Prior to regression analysis, θ_{eb} is calculated (a) with T_b and subcloud pressure held constant or (b) with q_b and subcloud pressure held constant.

the effects of removing Niño-3.4 variability and of performing analyses for local summer instead of the full calendar year (cf. Fig. 2a).

The regression analyses for the South Asian precipitation produced patterns of regression coefficients that were more spatially extensive for θ_{eb} than for q_b or T_b (cf. Figs. 2b, 6b, and 7b). To show why, we calculate θ_{eb} allowing only q_b or T_b to vary and then repeat the regression analysis (subcloud pressure is held constant in both of these alternate calculations of θ_{eb}). When only q_b is allowed to vary in the calculation of θ_{eb}, the pattern of regression coefficients closely matches that computed using the true θ_{eb} field (cf. Figs. A5a and 2b). This indicates that the exponential dependence of θ_e on q can account for the differences between Figs. 2b and 6b. When only T_b varies in the calculation of θ_{eb}, the regression pattern closely resembles that of observed T_b onto precipitation (cf. Figs. A5b and 7b), consistent with the linear relationship between θ_e and T.

REFERENCES

Adler, R. F., and Coauthors, 2003: The version-2 Global Precipitation Climatology Project (GPCP) monthly precipitation analysis (1979–present). *J. Hydrometeor.,* **4,** 1147–1167.

Arakawa, A., 2004: The cumulus parameterization problem: Past, present, and future. *J. Climate,* **17,** 2493–2525.

——, and W. H. Schubert, 1974: Interaction of a cumulus cloud ensemble with large-scale environment, Part I. *J. Atmos. Sci.,* **31,** 674–701.

Biasutti, M., I. M. Held, A. H. Sobel, and A. Giannini, 2008: SST forcings and Sahel rainfall variability in simulations of the twentieth and twenty-first centuries. *J. Climate,* **21,** 3471–3486.

——, A. H. Sobel, and S. J. Camargo, 2009: The role of the Sahara low in summertime Sahel rainfall variability and change in the CMIP3 models. *J. Climate,* **22,** 5755–5771.

Blanford, H., 1884: On the connexion of the Himalaya snowfall with dry winds and seasons of drought in India. *Proc. Roy. Soc. London,* **37,** 3–22.

Bollasina, M., and S. Nigam, 2011: The summertime "heat" low over Pakistan/northwestern India: Evolution and origin. *Climate Dyn.,* **37,** 957–970.

Boos, W. R., and K. A. Emanuel, 2008a: Wind–evaporation feedback and abrupt seasonal transitions of weak, axisymmetric Hadley circulations. *J. Atmos. Sci.,* **65,** 2194–2214.

——, and ——, 2008b: Wind–evaporation feedback and the axisymmetric transition to angular momentum-conserving Hadley flow. *J. Atmos. Sci.,* **65,** 3758–3778.

——, and Z. M. Kuang, 2010: Dominant control of the South Asian monsoon by orographic insulation versus plateau heating. *Nature,* **463,** 218–222.

——, and J. V. Hurley, 2013: Thermodynamic bias in the multimodel mean boreal summer monsoon. *J. Climate,* **26,** 2279–2287.

Box, G. E. P., J. M. Jenkins, and G. C. Reinsel, 1994: *Time Series Analysis: Forecasting and Control.* Prentice-Hall, 592 pp.

Bretherton, C. S., M. E. Peters, and L. E. Back, 2004: Relationships between water vapor path and precipitation over the tropical oceans. *J. Climate,* **17,** 1517–1528.

Brown, R. G., and C. S. Bretherton, 1997: A test of the strict quasi-equilibrium theory on long time and space scales. *J. Atmos. Sci.,* **54,** 624–638.

Caminade, C., and L. Terray, 2010: Twentieth century Sahel rainfall variability as simulated by the ARPEGE AGCM, and future changes. *Climate Dyn.,* **35,** 75–94.

Chakraborty, A., R. S. Nanjundiah, and J. Srinivasan, 2006: Theoretical aspects of the onset of Indian summer monsoon from perturbed orography simulations in a GCM. *Ann. Geophys.,* **24,** 2075–2089.

Charney, J. G., 1975: Dynamics of deserts and drought in Sahel. *Quart. J. Roy. Meteor. Soc.,* **101,** 193–202.

Chou, C., and J. D. Neelin, 2003: Mechanisms limiting the northward extent of the northern summer monsoons over North America, Asia, and Africa. *J. Climate,* **16,** 406–425.

——, ——, and H. Su, 2001: Ocean-atmosphere-land feedbacks in an idealized monsoon. *Quart. J. Roy. Meteor. Soc.,* **127,** 1869–1891.

Climate Prediction Center, cited 2011: Monthly Niño 3.4 SST anomalies. [Available online at http://www.esrl.noaa.gov/psd/data/climateindices/list/.]

Colman, R. A., A. F. Moise, and L. I. Hanson, 2011: Tropical Australian climate and the Australian monsoon as simulated by 23 CMIP3 models. *J. Geophys. Res.,* **116,** D10116, doi:10.1029/2010JD015149.

Compo, G. P., and P. D. Sardeshmukh, 2010: Removing ENSO-related variations from the climate record. *J. Climate,* **23,** 1957–1978.

Derbyshire, S. H., I. Beau, P. Bechtold, J. Y. Grandpeix, J. M. Piriou, J. L. Redelsperger, and P. M. M. Soares, 2004: Sensitivity of moist convection to environmental humidity. *Quart. J. Roy. Meteor. Soc.,* **130,** 3055–3079.

Douglas, M. W., R. A. Maddox, K. Howard, and S. Reyes, 1993: The Mexican monsoon. *J. Climate,* **6,** 1665–1677.

Douville, H., F. Chauvin, and H. Broqua, 2001: Influence of soil moisture on the Asian and African monsoons. Part I: Mean monsoon and daily precipitation. *J. Climate,* **14,** 2381–2403.

Eltahir, E. A. B., 1998: A soil moisture rainfall feedback mechanism. 1. Theory and observations. *Water Resour. Res.,* **34,** 765–776.

——, and C. L. Gong, 1996: Dynamics of wet and dry years in West Africa. *J. Climate,* **9,** 1030–1042.

Emanuel, K. A., 1994: *Atmospheric Convection.* Oxford University Press, 580 pp.

——, 1995: On thermally direct circulations in moist atmospheres. *J. Atmos. Sci.,* **52,** 1529–1534.

——, J. D. Neelin, and C. S. Bretherton, 1994: On large-scale circulation in convecting atmospheres. *Quart. J. Roy. Meteor. Soc.,* **120,** 1111–1143.

Fasullo, J., and P. J. Webster, 2003: A hydrological definition of Indian monsoon onset and withdrawal. *J. Climate,* **16,** 3200–3211.

Gan, M. A., V. E. Kousky, and C. F. Ropelewski, 2004: The South America monsoon circulation and its relationship to rainfall over west-central Brazil. *J. Climate,* **17,** 47–66.

Garreaud, R. D., and J. M. Wallace, 1998: Summertime incursions of midlatitude air into subtropical and tropical South America. *Mon. Wea. Rev.,* **126,** 2713–2733.

Giannini, A., R. Saravanan, and P. Chang, 2003: Oceanic forcing of Sahel rainfall on interannual to interdecadal time scales. *Science,* **302,** 1027–1030.

Gill, A. E., 1980: Some simple solutions for heat-induced tropical circulation. *Quart. J. Roy. Meteor. Soc.,* **106,** 447–462.

Godfred-Spenning, C. R., and C. J. C. Reason, 2002: Interannual variability of lower-tropospheric moisture transport during the Australian monsoon. *Int. J. Climatol.,* **22,** 509–532.

Gutzler, D. S., 2004: An index of interannual precipitation variability in the core of the North American monsoon region. *J. Climate,* **17,** 4473–4480.

Haarsma, R. J., F. M. Selten, S. L. Weber, and M. Kliphuis, 2005: Sahel rainfall variability and response to greenhouse warming. *Geophys. Res. Lett.,* **32,** L17702, doi:10.1029/2005GL023232.

Hoerling, M., J. Hurrell, J. Eischeid, and A. Phillips, 2006: Detection and attribution of twentieth-century northern and southern African rainfall change. *J. Climate,* **19,** 3989–4008.

Janowiak, J. E., 1988: An investigation of interannual rainfall variability in Africa. *J. Climate,* **1,** 240–255.

JISAO, cited 2011: University of Delaware global surface air temperature and precipitation climatology and monthly grids, 1900–2008. [Available online at http://jisao.washington.edu/datasets/ud/.]

Kalnay, E., and Coauthors, 1996: The NCEP/NCAR 40-Year Reanalysis Project. *Bull. Amer. Meteor. Soc.,* **77,** 437–471.

Li, Y., R. Y. Lu, and B. W. Dong, 2007: The ENSO–Asian monsoon interaction in a coupled ocean–atmosphere GCM. *J. Climate,* **20,** 5164–5177.

Lindzen, R. S., and A. Y. Hou, 1988: Hadley circulations for zonally averaged heating centered off the equator. *J. Atmos. Sci.,* **45,** 2416–2427.

Lu, J., 2009: The dynamics of the Indian Ocean sea surface temperature forcing of Sahel drought. *Climate Dyn.,* **33,** 445–460.

Matsuno, T., 1966: Quasi-geostrophic motions in the equatorial area. *J. Meteor. Soc. Japan,* **44,** 25–42.

Matsuura, K., and C. J. Willmott, cited 2011: Terrestrial precipitation: 1900-2008 gridded monthly time series. Center for Climatic Research Rep. [Available online at http://climate.geog.udel.edu/~climate/html_pages/Global2_Ts_2009/README.global_p_ts_2009.html.]

McHugh, M. J., 2004: Near-surface zonal flow and East African precipitation receipt during austral summer. *J. Climate,* **17,** 4070–4079.

Neelin, J. D., 2007: Moist dynamics of tropical convection zones in monsoons, teleconnections and global warming. *The Global Circulation of the Atmosphere,* T. Schneider and A. H. Sobel, Eds., Princeton University Press, 267–301.

——, and N. Zeng, 2000: A quasi-equilibrium tropical circulation model—Formulation. *J. Atmos. Sci.,* **57,** 1741–1766.

——, O. Peters, J. W. B. Lin, K. Hales, and C. E. Holloway, 2008: Rethinking convective quasi-equilibrium: Observational constraints for stochastic convective schemes in climate models. *Philos. Trans. Roy. Soc.,* **366A,** 2581–2604.

Nie, J., W. R. Boos, and Z. M. Kuang, 2010: Observational evaluation of a convective quasi-equilibrium view of monsoons. *J. Climate,* **23,** 4416–4428.

Peterson, T. C., and R. S. Vose, 1997: An overview of the global historical climatology network temperature database. *Bull. Amer. Meteor. Soc.,* **78,** 2837–2849.

Peyrillé, P., and J. P. Lafore, 2007: An idealized two-dimensional framework to study the West African monsoon. Part II: Large-scale advection and the diurnal cycle. *J. Atmos. Sci.,* **64,** 2783–2803.

Prive, N. C., and R. A. Plumb, 2007a: Monsoon dynamics with interactive forcing. Part I: Axisymmetric studies. *J. Atmos. Sci.,* **64,** 1417–1430.

——, and ——, 2007b: Monsoon dynamics with interactive forcing. Part II: Impact of eddies and asymmetric geometries. *J. Atmos. Sci.,* **64,** 1431–1442.

Ramage, C. S., 1966: The summer atmospheric circulation over the Arabian Sea. *J. Atmos. Sci.,* **23,** 144–150.

Rasmusson, E. M., and T. H. Carpenter, 1983: The relationship between eastern equatorial Pacific sea surface temperatures and rainfall over India and Sri Lanka. *Mon. Wea. Rev.,* **111,** 517–528.

Raymond, D. J., and X. Zeng, 2000: Instability and large-scale circulations in a two-column model of the tropical troposphere. *Quart. J. Roy. Meteor. Soc.,* **126,** 3117–3135.

Robock, A., M. Q. Mu, K. Vinnikov, and D. Robinson, 2003: Land surface conditions over Eurasia and Indian summer monsoon rainfall. *J. Geophys. Res.,* **108,** 4131, doi:10.1029/2002JD002286.

Rodwell, M. J., and B. J. Hoskins, 1996: Monsoons and the dynamics of deserts. *Quart. J. Roy. Meteor. Soc.,* **122,** 1385–1404.

Rowell, D. P., 2003: The impact of Mediterranean SSTs on the Sahelian rainfall season. *J. Climate,* **16,** 849–862.

Saji, N. H., B. N. Goswami, P. N. Vinayachandran, and T. Yamagata, 1999: A dipole mode in the tropical Indian Ocean. *Nature,* **401,** 360–363.

Shukla, J., and D. A. Paolino, 1983: The southern oscillation and long-range forecasting of the summer monsoon rainfall over India. *Mon. Wea. Rev.,* **111,** 1830–1837.

Smith, T. M., and R. W. Reynolds, 2004: Improved extended reconstruction of SST (1854–1997). *J. Climate,* **17,** 2466–2477.

Taschetto, A. S., C. C. Ummenhofer, A. Sen Gupta, and M. H. England, 2009: Effect of anomalous warming in the central Pacific on the Australian monsoon. *Geophys. Res. Lett.,* **36,** L12704, doi:10.1029/2009GL038416.

——, R. J. Haarsma, A. Sen Gupta, C. C. Ummenhofer, K. J. Hill, and M. H. England, 2010: Australian monsoon variability driven by a Gill–Matsuno-type response to central west Pacific warming. *J. Climate,* **23,** 4717–4736.

Thorncroft, C. D., and M. Blackburn, 1999: Maintenance of the African easterly jet. *Quart. J. Roy. Meteor. Soc.,* **125,** 763–786.

——, N. Hanh, C. D. Zhang, and P. Peyrille, 2011: Annual cycle of the West African monsoon: Regional circulations and associated water vapour transport. *Quart. J. Roy. Meteor. Soc.,* **137,** 129–147.

Tompkins, A. M., 2001: Organization of tropical convection in low vertical wind shears: The role of water vapor. *J. Atmos. Sci.,* **58,** 529–545.

Trenberth, K. E., and D. J. Shea, 2005: Relationships between precipitation and surface temperature. *Geophys. Res. Lett.,* **32,** L14703, doi:10.1029/2005GL022760.

——, D. P. Stepaniak, and J. M. Caron, 2000: The global monsoon as seen through the divergent atmospheric circulation. *J. Climate,* **13,** 3969–3993.

Uppala, S. M., and Coauthors, 2005: The ERA-40 Re-Analysis. *Quart. J. Roy. Meteor. Soc.,* **131,** 2961–3012.

Vera, C., and Coauthors, 2006: Toward a unified view of the American monsoon systems. *J. Climate,* **19,** 4977–5000.

Vernekar, A. D., J. Zhou, and J. Shukla, 1995: The effect of Eurasian snow cover on the Indian monsoon. *J. Climate,* **8,** 248–266.

Wang, B., and Z. Fan, 1999: Choice of South Asian summer monsoon indices. *Bull. Amer. Meteor. Soc.,* **80,** 629–638.

——, and Q. H. Ding, 2008: Global monsoon: Dominant mode of annual variation in the tropics. *Dyn. Atmos. Oceans,* **44,** 165–183.

Webster, P. J., V. O. Magana, T. N. Palmer, J. Shukla, R. A. Tomas, M. Yanai, and T. Yasunari, 1998: Monsoons: Processes, predictability, and the prospects for prediction. *J. Geophys. Res.,* **103** (C7), 14 451–14 510.

——, A. M. Moore, J. P. Loschnigg, and R. R. Leben, 1999: Coupled ocean–atmosphere dynamics in the Indian Ocean during 1997–98. *Nature,* **401,** 356–360.

Yang, S., and K. M. Lau, 2004: Interannual variability of the Asian monsoon. *Asian Monsoon,* B. Wang, Ed., Springer-Praxis, 259–293.

Zhang, C. D., D. S. Nolan, C. D. Thorncroft, and H. Nguyen, 2008: Shallow meridional circulations in the tropical atmosphere. *J. Climate,* **21,** 3453–3470.